Up-to-downwave asymmetry of the CFOSAT SWIM fluctuation spectrum for wave direction ambiguity removal

Huimin Li, Danièle Hauser, Bertrand Chapron, Frédéric Nouguier, Patricia Schippers, Biao Zhang, Jingsong Yang, Yijun He

Up-to-downwave asymmetry of the CFOSAT SWIM fluctuation spectrum for wave direction ambiguity removal

Huimin Li, Danièle Hauser, Bertrand Chapron, Frédéric Nouguier, Patricia Schippers, Biao Zhang, Jingsong Yang and Yijun He

***Abstract*—The surface waves investigation and monitoring (SWIM) aboard the China-France Oceanography Satellite (CFOSAT), a pioneer conically scanning wave spectrometer, was successfully launched on October 29, 2018. Its innovative configuration composed of one nadir and 5 rotating near-nadir beams is designed to simultaneously observe the significant wave height as well as the directional wave spectrum at global scale. In this study, we examine the two-dimensional fluctuation spectrum of the three spectral beams (θ = 6°,8°,10°) by combining all the azimuth directions within one entire rotation of 360°. Spectral analysis of the radar backscattering profile along each azimuth is systematically carried out using the periodogram technique. The obtained fluctuation spectrum is consistent with the collocated wave slope spectra in terms of the qualitative wave features. Moreover, a quantitative up-to-downwave asymmetry of the fluctuation spectrum is documented with larger spectral level in the upwave direction for all the three spectral beams. Magnitude of the defined up-to-downwave spectral ratio are mostly greater than 1 with the down-to-upwave ratio smaller than 1. This asymmetry characteristics can be readily utilized to remove the 180° wave direction ambiguity from a practical point of view. The preliminary results demonstrate that the 10° beam shows better performance in comparison to the other two beams. This shall lay strong basis for the operational implementation of such algorithm to resolve the direction ambiguity.**

This work is supported in part by the National Key Research and Development Program of China (under Grant 2016YFC1401002 and 2016YFC1401005), by Centre National d'études Spatiales (CNES) under the TOSCA program, by the Startup Foundation for Introducing Talent of NUIST, by the National Natural Science Foundation (under Grant 42006163 and 41620104003), by the European Space Agency and Ministry of Science and Technology Dragon 5 Cooperation Programme (ID. 58009).

Huimin Li is with School of Marine Sciences, Nanjing University of Information Science and Technology, Nanjing 210044, China and State Key Laboratory of Satellite Ocean Environment Dynamics, Second Institute of Oceanography, Ministry of Natural Resources, Hangzhou 310012, China. (E-mail: huimin.li@nuist.edu.cn).

Danièle Hauser is with Laboratoire Atmosphère, Milieux, Observations Spatiales (LATMOS), Université Paris-Saclay, UVSQ, Centre National de la Recherche Scientifique (CNRS), Sorbonne Université, 78280 Guyancourt, France (e-mail: daniele.hauser@latmos.ipsl.fr).

Bertrand Chapron and Frédéric Nouguier are with IFREMER, Univ. Brest, CNRS, IRD, Laboratoire d'Océánographie Physique et Spatiale (LOPS), Plouzane 29280, France (E-mail: bertrand.chapron@ifremer.fr; frederic.nouguier@ifremer.fr).

Biao Zhang and Yijun He are with School of Marine Sciences, Nanjing University of Information Science and Technology, Nanjing 210044, China. (E-mail: zhangbiao@nuist.edu.cn; yjhe@nuist.edu.cn).

Patricia Schippers is with the ACRI-ST company, Guyancourt, France (Email: patricia.schippers@latmos.ipsl.fr).

Jingsong Yang is with the State Key Laboratory of Satellite Ocean Environment Dynamics, Second Institute of Oceanography, Ministry of Natural Resources, Hangzhou 310012, China (Email: jsyang@sio.org.cn).

Manuscript received xx xx, 2020; revised xx xx, 2020.

***Index Terms*—CFOSAT SWIM; Up-to-downwave asymmetry of fluctuation spectrum; Wave direction ambiguity removal**

I. INTRODUCTION

OCEAN waves are important upper ocean processes to regulate the heat, momentum exchange of the air-sea interaction. Since the directional wave spectrum is able to fully characterize the sea state, its observations are essential for wave related studies. Until recently, *in-situ* buoys and spaceborne synthetic aperture radar (SAR) have been the chief source of wave spectra measurements [1]. Yet, limitations of these techniques are also evident due to either the restricted spatial coverage of buoys or the nonlinear loss of wave information of SAR imaging [2]. An innovative technique is necessary to complement the existing manners for accurate and comprehensive observations of directional wave spectrum at the global scale.

Radars operating at near-nadir incidence angles rely on the wave slope induced variations in the returned signal to measure the ocean waves. A conically scanning antenna receives backsatter at various azimuth angles to resolve the two-dimensional wave field. Such concept of a wave spectrometer has been proposed for over 30 years [3]. Its capability to observe the directional wave spectrum was then evidenced by multiple airborne experiments [4], [5]. One of the two payloads aboard the China-France Oceanography Satellite (CFOSAT), surface wave investigation and monitoring (SWIM) is such a wave spectrometer. The instrument characteristics as well as the forward simulation of SWIM backscattering have been detailed to support the mission design [6], [7]. The successful launch of CFOSAT marks the first ever deployment of a conically scanning real aperture radar (RAR) in the space [8], [9]. This shall facilitate the investigation of global ocean waves, not only regarding the wave height, but also the wave directional spectra to characterize the complex sea state [9]. It is expected to help advance our understanding of wind-wave interactions at global scale [10] as well as to refine the accuracy of numerical modeling [11], [12].

SWIM operates at Ku-band with the center radar frequency at 13.575 GHz [7]. It has six beams with 1 nadir and 5 near-nadir incidence angles (0°,2°,4°,6°,8°,10°). The nadir beam is similar to a state-of-the-art altimeter in purpose to measure both the significant wave height and the wind speed. The five near-nadir beams sequentially illuminates the sea

surface at different azimuth angles. Each beam employs a chirp signal of 320 MHz for range detection along given azimuth. Spectral analysis of the backscattering profile along the range is conducted to obtain the modulation spectrum in that azimuth. Inversion of the wave height spectrum in this azimuth direction follows. The two-dimensional wave spectra is then accordingly constructed by combining all azimuth directions within one rotation across the entire 360°.

At such low incidence angle as SWIM does, radar backscattering of the sea surface is dominated by the quasi-specular reflection from the wave slope satisfying the specular condition [13]. The geometrical modulation is the dominant mechanism for the signal contrast modulation. It is due to the change of local incidence angle provoked by the tilt of the long wave slopes. Assuming that the mechanism is linear (true for small slopes) and the hydrodynamic modulation is negligible, the measured modulation spectrum is linearly related to the waves slope spectrum via the tilt modulation transfer function (MTF). Under the approximation of small curvature effects, the backscattering at near-nadir incidence is proportional to the wave slope probability density function (PDF), the tilt MTF, the derivative of backscattering, is then related to the wave slope PDF. Most of the simulation studies presumed the wave slope spectrum to be Gaussian and isotropic, producing the simulated polar-symmetric modulation spectrum [6]. However, it has been reported that the modulation spectrum derived from the airborne observations was actually not symmetric [3]. They speculated that this is possibly due to the non-isotropic nature of wave slopes PDF and/or the second-order hydrodynamic modulation. However, no statistical analysis was presented due to the limited number of aircraft measurements in that paper [3]. In the meanwhile, many studies have disclosed that the up-downwave wave slope follows a non-Gaussian shape based on both the sun glitter and the near-nadir microwave radar measurements [14], [15], [16], [17]. In other words, the derivative of wave slope PDF differs from upwave (or upwind) to downwave (or downwind) direction. The MTF variation relative to the wave directions might contradict with previous results of polar-symmetric modulation spectrum. In fact, the tilt MTF estimated based on the Global Precipitation Mission data has demonstrated the azimuthal dependence of MTF with larger values in the upwave (or upwind) [18].

As a matter of fact, it is the fluctuation spectrum that is directly calculated from the backscattering profile rather than the modulation spectrum. These two spectra are related through the radar impulse response spectrum as well as the speckle noise spectrum [3], [4]. In contrast to a fixed antenna configuration, the rotating beams of SWIM allow to observe the sea surface at various azimuth directions. The direct comparison of fluctuation spectrum between the upwave and downwave direction becomes therefore feasible. In this study, SWIM observations are collocated with the directional wave spectra from WaveWatch III (WW3), and the dominant direction of the WW3 spectra are used as reference in the following analysis. Up-to-downwave asymmetry of the fluctuation spectrum is documented through comparison of the values at peak pairs with 180° ambiguity. Note that one of the unsolved issue in the present SWIM data processing chain is the removal of the wave direction ambiguity [9]. We then present the preliminary results for removing the wave direction ambiguity by taking advantage of this up-to-downwave asymmetry.

The rest of this paper is organized as follows. Section II details the SWIM data included in this study as well as the spectral analysis to obtain the fluctuation spectrum. The up-to-downwave asymmetry of fluctuation spectrum is presented in Section III and the preliminary results for direction ambiguity removal is given in Section IV. Discussion and conclusion then follow in Section IV.

II. DATA AND METHOD

In this section, we first present the SWIM observations used in this paper as well as the collocated ancillary data, including ocean wave spectra and wind field. The spectral analysis method of periodogram to calculate the fluctuation spectrum for each azimuth direction then follows.

A. SWIM observations and ancillary data

SWIM is a pioneer Ku-band RAR developed based on the concept detailed in [19]. It measures the radar backscattering with 6 beams at incidence angle from 0° to 10° with the increment of 2°. It is deployed in the orbit at an altitude about 500 km. The observation swaths in radius rely on the incidence angle, for example, the 10° beam has a swath in radius of 90 km. Radar footprint of the near-nadir beams is about 18 km by 18 km on the ground with the original slant range resolution of 0.47 m. Since a certain number of range bins and azimuth samples needs to be averaged on board to reduce the downlink rate, the slant range resolution decreases to 0.9 m or 1.5 m depending on the number of averaged bins. More details of SWIM instrument parameters can be referred to [7].

Each of the near-nadir beams rotates at a speed of 5.6 rpm to cover all azimuth angles with a directional sampling about 7.5°. It should be noted that at any given moment, the 5 near-nadir beams are not contiguous in azimuth angles due to the mechanical constraints in the rotating plate (see Figure 2 in [7]). The near-nadir beams of 6°,8°,10° are dedicated to the measurements of directional wave spectra, which are often termed as spectral beams. The other two near-nadir beams of 2° and 4° are mainly kept to provide the backscattering profile relative to the incidence angle. Fig. 1 presents an example of the acquisition pattern of the nadir and 6°,8°,10° beams within two entire rotations. In this study, we define one rotation covering the entire 360° to start from the azimuth direction closest to 270° clockwise from the true North. Over one beam rotation about 10.8 s, the characteristics of ocean waves being measured could be reasonably assumed to remain unchanged under low to moderate wind/wave conditions. Therefore, all the azimuth directions within one rotation can then be combined to construct the two-dimensional fluctuation spectrum.

Numerous studies have demonstrated that at small incidence angle as SWIM operates, the radar backscattering is dominated by the quasi-specular reflection from the wave facets perpendicular to the radar line-of sight [13], [20]. According to [7],

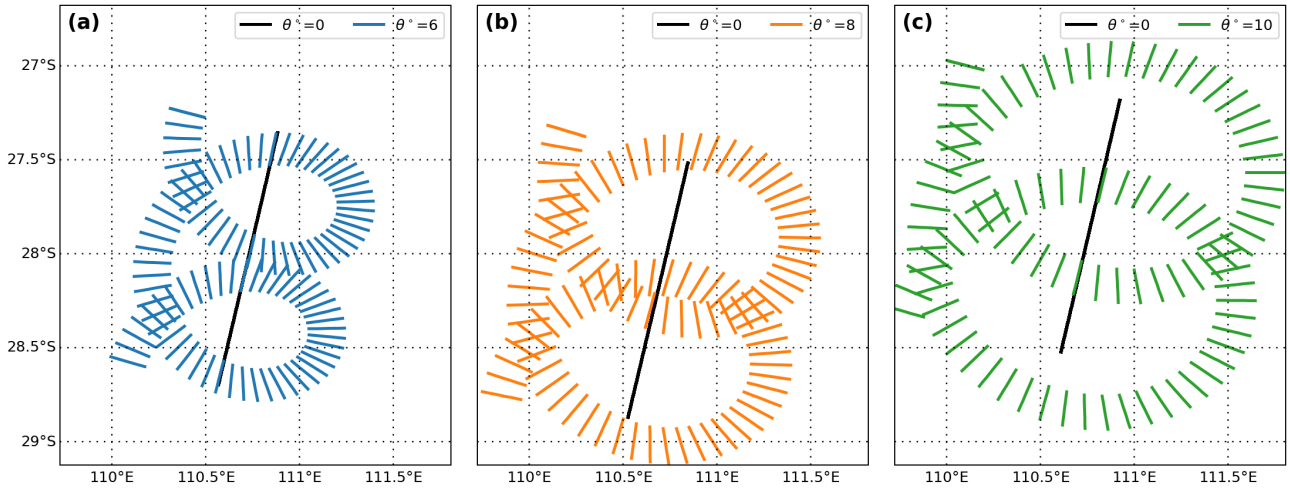

Fig. 1. An example for acquisition pattern of (a) 6°, (b) 8° and (c) 10° beams within two rotations of 360°. Black curve denotes footprint of the nadir beam. Note that the slightly varying coverage of these three incidence angles is due to their incontiguous azimuth directions at given moment.

[13], the modulation spectrum of the radar backscatter can then be written as

$$P_M(k,\phi) = \frac{2\pi}{L_y}\left(cot\theta - \frac{\partial ln\sigma_0}{\partial\theta}\right)^2 k^2 F(k,\phi) \qquad (1)$$

where L_y is a length related to the azimuthal width of the beam footprint referred to Eq.(9) in [7]. $F(k,\phi)$ is the two-dimensional wave height spectrum and σ^0 is the SWIM-received normalized radar cross-section (NRCS and σ^0 used interchangeably in this paper). As concluded in [3], the hydrodynamic modulation and nonlinear wave-wave interactions are solely of second-order effect and can be neglected at such near-nadir incidence angles. The modulation spectrum is associated with the fluctuation spectrum directly estimated from the backscattering signal by

$$P_F(k,\phi) = P_{IR}(k)P_M(k,\phi) + P_{sp}(k) \qquad (2)$$

where $P_{IR}(k)$ is the impulse response spectrum and $P_{sp}(k)$ denotes the speckle spectrum. As annotated, these two spectra are usually assumed to be centro-symmetric across one rotation of 360° [9]. This makes the up-to-downwave contrast of the fluctuation spectrum comparable to that of $P_M(k,\phi)$. Since this paper does not focus on inversion of the wave spectrum, up-to-downwave asymmetry of only the fluctuation spectrum is investigated unless otherwise stated.

In this study, we utilized the SWIM observations acquired on 21 October, 2019, which are processed with the updated on-board migration compensation algorithm [9]. The ocean wave spectra output from the WaveWath III (WW3) forecast is collocated to be the reference wave direction. The WW3 directional wave spectra are available at the spatial resolution of 0.5° every 30 minutes. The WW3 wave spectrum is composed of 24 directions and 32 frequencies in the range of 0.037 Hz to 0.7 Hz, covering the SWIM resolved wavelength range from 70 m to 500 m. Forecast winds from the European Centre for Medium-Range Weather Forecasts (ECMWF) are also included to examine the possible wind speed dependence of the spectral asymmetry, which are available at a spatial resolution of 0.25° every 3 hours. Both WW3 and ECMWF products are collocated with the center of each SWIM rotation in terms of the nearest spatial and temporal distance.

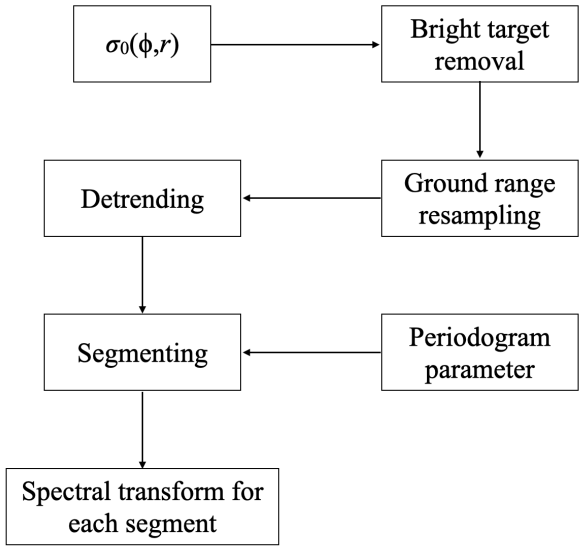

Fig. 2. Flowchart of the fluctuation spectrum estimate along each azimuth direction. The ground range resampling spacing is set to be 5 m and the periodogram window is 512 pixels with 256 pixels overlapping.

B. Spectral analysis

In this study, the spectral analysis for the three beams of 6°, 8°, 10° is systematically carried out with the algorithm flowchart for the fluctuation spectrum at each azimuth given in Fig. 2. Since targets such as ships or platforms could cause very high backscattering signal, the pixels with NRCS larger than 99% percentile of that azimuth are replaced by the averaged value. The slightly varying incidence angle from the near range to the far range results in an irregular ground range sampling. A preprocessing step is thus performed to resample

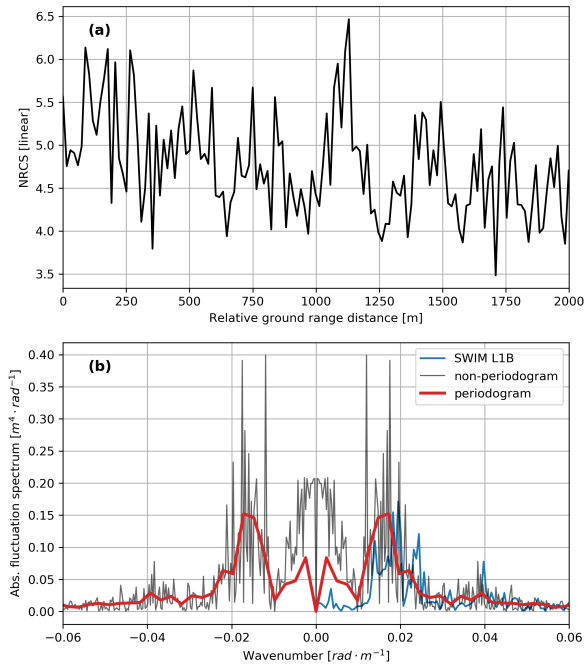

Fig. 3. An example for (a) SWIM measured NRCS profile of 10° beam with respect to the relative ground range distance; (b) Comparison of the obtained fluctuation spectrum using periodogram algorithm in Fig. 2 (red curve) and non-periodogram method (black curve) and the results annotated in SWIM level-1B products (blue curve).

the signal onto a constant ground range grid. Throughout this study, the ground range resampling is set to be 5 m for all three spectral beams. The detrending is conceived with a low-pass Gaussian filtering to estimate the overall trend of backscattering profile along the range. In order to reduce the noise effect, the periodogram technique is employed. The signal fluctuations $\delta\sigma_0$ profile is divided into segments at lengths of 512 pixels with half overlapping. This leads to 15 segments for each azimuth direction and one averaged spectrum is obtained in the end. Note that this algorithm differs from that used in the level-2 processing chain by two aspects. On one hand, this algorithm takes advantage of the segments and periodogram to reduce speckle noise effect. On the other hand, we use rotations of 360° rather than box in the level-2 products, in order to facilitate the up-to-downwave comparison.

An example of the σ_0 profile along the relative ground range distance is given in Fig. 3(a). A decreasing trend of NRCS is evident, which is removed by the detrending step in Fig. 3 prior to the fluctuation spectrum estimate. The fluctuation spectra obtained using different methods are shown in Fig. 3(b). The thin black curve denotes the fluctuation spectrum calculated by the genuine Fourier Transform (FT) of the NRCS profile, which is quite noisy with high spectral signal at the low frequencies. For comparison, the fluctuation spectrum provided in the SWIM level-1b product is plotted as the blue curve. In this latter case, the FT was applied on the full-length segment (limit to the window where the signal-to-noise ratio is higher than 3 dB), and the output spectrum is averaged over two consecutive wavenumbers. With our periodogram method as well as the averaged spectrum over multiple segments, the spectrum is less noisy and the signature is more clearer. As a result, we choose to compute the fluctuation spectrum along a given azimuth direction using the periodogram method in the rest of this paper unless particularly stated. Note that in calculating the fluctuation spectrum, the resampled ground range spacing is 5 m and the periodogram size of 512 pixel is used, resulting in the wavenumber bin of 0.00245437 $rad \cdot m^{-1}$.

III. UP-TO-DOWNWAVE ASYMMETRY OF FLUCTUATION SPECTRUM

In this section, a two-dimensional fluctuation spectrum computed using the periodogram method is first displayed and discussed as a representative example. The up-to-downwave asymmetry of the fluctuation spectrum between the two wave peaks with 180° ambiguity is then presented from a statistical point of view.

A. Case study

The two-dimensional fluctuation spectrum is systematically constructed over one beam rotation of 360°. In general, there are approximately 50 azimuth directions within one rotation for each beam. Examples of the obtained directional fluctuation spectrum at positive wavenumbers are shown in Fig. 4 for the three spectral beams of 6°, 8°, 10°, respectively. Its counterpart at the negative wavenumber (not shown) is simply a replica of the pattern at the positive wavenumber. Note that the angular sector within ±15° along the track direction is mostly contaminated by high speckle noise, which usually conceals the actual wave signal [9]. As such, this sector is simply masked out in the following analyses. The three beams display quite similar spectral signatures with one dominant wave system at wavelength around 400 m. In the quantitative terms, the 6° beam has the largest spectral magnitude, while the 10° is the smallest. This decreasing spectral level might be partly associated with the impulse response function and the more significant contribution of speckle noise at 6° due to fewer data points for the fluctuation spectrum estimate.

As shown in Fig. 4(a)-(c), the spectral peaks position at 60° and 240° with the 180° ambiguity. By comparison, magnitude of the fluctuation spectrum appears to be smaller at the 60° peak than the 240° peak. Such contrast is more evident for the 10° beam in Fig. 4(c). To determine the relative wave direction, the collocated WW3 wave slope spectra is shown in Fig. 4(d). The dominant wavelength is in good agreement with that of the fluctuation spectra for all three spectral beams. According to the WW3 wave spectra, the peak waves propagate towards the northeast direction. As such, the spectral peak at 60° in Fig.4(a)-(c) corresponds to the downwave where the radar looking is in alignment with the wave traveling direction. While the peak at 240° correspond to the upwave direction, where the radar line-of-sight direction is opposite to the wave propagation direction. Based on this case study, we found that the fluctuation spectra at downwave exhibits smaller magnitude than that at the upwave direction.

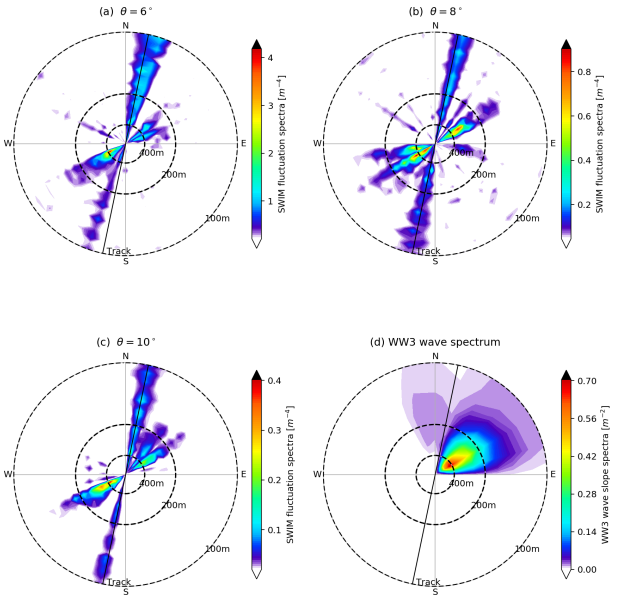

Fig. 4. Two-dimensional fluctuation spectrum constructed from one rotation of 360° for the beam of (a) 6°, (b) 8° and (c) 10°. The collocated WW3 wave slope spectrum is shown in (d) for comparison. The WW3 spectra direction corresponds to the direction that the waves travel to.

As a preparation to further statistics of the up-to-downave spectrum contrast, the spectral peak pairs with 180° ambiguity are consistently detected. Fig. 6 presents the flowchart to search for the valid peak pairs and to compute the averaged fluctuation spectrum over the detected peaks. Local peaks are identified based on the constructed two-dimensional fluctuation spectrum, among which the peak pairs are determined with their wavelength difference smaller than 0.0147 $rad{\cdot}m^{-1}$ and their direction difference within 180±30°. For each pair, the fluctuation spectra profile along the peak direction is extracted relative to the wavenumber. Fig. 5 illustrates such extracted profiles from the fluctuation spectra shown in Fig. 4 for the three incidence angles. It is worth noting that the fluctuation spectral magnitude near the peaks is much higher than the speckle noise level reported in [9], which is reproduced as the green horizontal lines in Fig. 5. The wavenumber range over which to calculate the spectrum average is determined by the 3-dB bandwidth of each profile. This range is marked by the vertical dashed lines in the same color with the corresponding curves. As shown in Fig. 5, the averaged spectral signal around the direction of 60° (blue curve) is smaller than that around 240°. In other words, the averaged spectrum at the downwave peak is lower in comparison to its ambiguous counterpart. In this case, the difference of averaged profile around the peaks within [0°, 180°] and within [180°, 360°] is negative as it represents the difference of downwave part relative to the upwave. Considering the magnitude of this difference relying on the absolute value of the fluctuation spectrum, it is not straightforward to reflect their statistical relativity. As an alternative, we define the ratio of spectral average over the peak ϕ_1 in [0°,180°] to ϕ_2 in [180°,360°], expressed as

$$RT_P = \frac{P_m(\phi_1)}{P_m(\phi_2)}, \phi_1 \in [0°, 180°], \phi_2 \in [180°, 360°] \quad (3)$$

RT_P is so defined that it is independent of the absolute spectral level. Here it is assumed that the peak spectral level is much higher than the speckle noise, which holds true for wave directions away from the track angle. RT_P represents the down-to-upwave ratio of averaged fluctuation spectrum when the true wave direction (traveling to) is within [0°,180°]. While it is the up-to-downwave ratio if the true wave direction falls within [180°,360°]. The wave direction shown in Fig. 4 is about 60° so that the RT_P denotes the down-to-upwave ratio for this case. As demonstrated in Fig. 5, RT_P varies relative to the SWIM incidence angles, with values of 0.51 for 6° beam, 0.93 for 8° beam and 0.61 for 10° beam. The fact that RT_P is smaller than one illustrates that for this selected case, the fluctuation spectrum is smaller in the downwave direction than in the upwave direction.

B. Statistics of fluctuation spectrum RT_P

Though the case in Fig. 4 has manifested the up-to-downwave asymmetry of the fluctuation spectrum, it is not yet plausible to conclude its generality. In order to examine this asymmetry from a statistical point of view, the two ambiguous directions of fluctuation spectrum need to be categorized into the relative wave directions. In this study, we associated the identified spectral peak pairs with the WW3 wave peaks in terms of the spectral distance, which is defined as [21]

$$SD = \frac{1}{60}\left(|D_1 - D_2| + 2 \times \frac{|T_1 - T_2|}{T_1 + T_2} \times 250\right) \quad (4)$$

where D_1,D_2 are the detected SWIM and the WW3 peak direction, respectively. T_1 and T_2 are the peak wave period in the unit of s. By definition, SD takes the impact of both wave period and the propagation direction into account to assess the similarity of two peaks. Factors of 60 and 250 are chosen to describe that 20° errors in direction are equivalent to 8% errors in the wave period. The peak pair is kept if either of the ambiguous peaks obtains the spectral distance smaller than 3 relative to its WW3 counterpart. There are initially 867, 1194, 1443 peak pairs identified based on the directional fluctuation spectrum. The criteria of spectral distance smaller than 3 leads to 647, 855, 975 pairs of 6°, 8° and 10° beams for the statistical analyses, respectively. Most of the eliminated spectral peaks locate at wavelengths longer than 600 m (not shown), which is beyond the detection range of SWIM.

To examine the asymmetry from a statistical point of view, the box plot of RT_P as defined by Eq.(3) is shown in Fig. 7 regarding the collocated WW3 peak wave direction. Note that the speckle noise spectrum constant is subtracted from the fluctuation spectrum to compute RT_P. As annotated in Fig. 5, the constants are 0.0105 m^{-4}, 0.007m^{-4}, 0.0055m^{-4} for the 6°, 8° and 10°, respectively. The up-to-downwave asymmetry is prominent for all three beams, featured by the RT_P either smaller or higher than 1. When ϕ lies in [0°,180°], RT_P corresponding to the down-to-upwave ratio is smaller than 1,

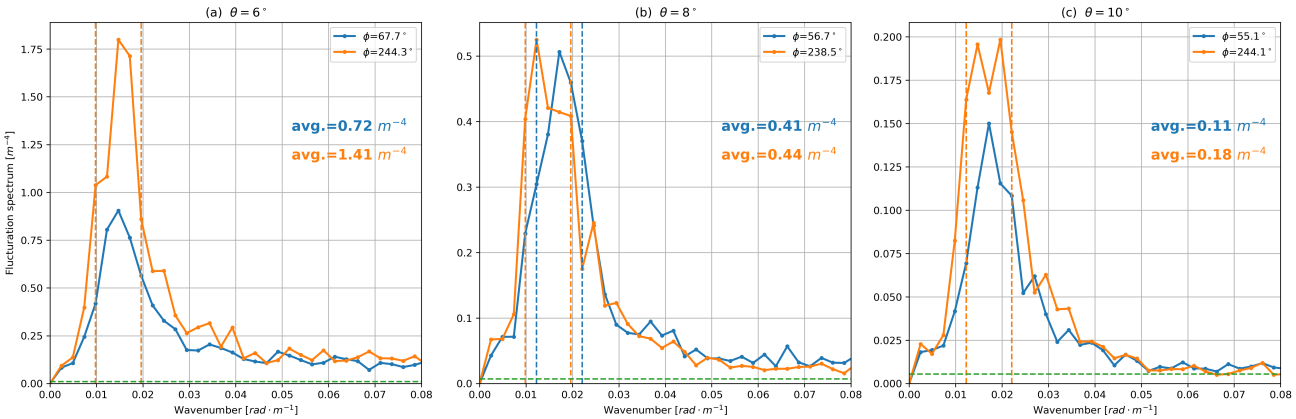

Fig. 5. Demonstration of the fluctuation spectral profile at the ambiguous peaks from the case shown in Fig. 4 for (a) 6°, (b) 8° and (c) 10° beams. The vertical dashed lines indicate the wavenumber range over which to calculate the averaged values. The averaged spectral magnitude is annotated in the same color with the curves. A constant for the speckle noise spectrum is reproduced based on [9] and plotted as the horizontal line in green, which is sufficiently small in comparison to the peak spectrum.

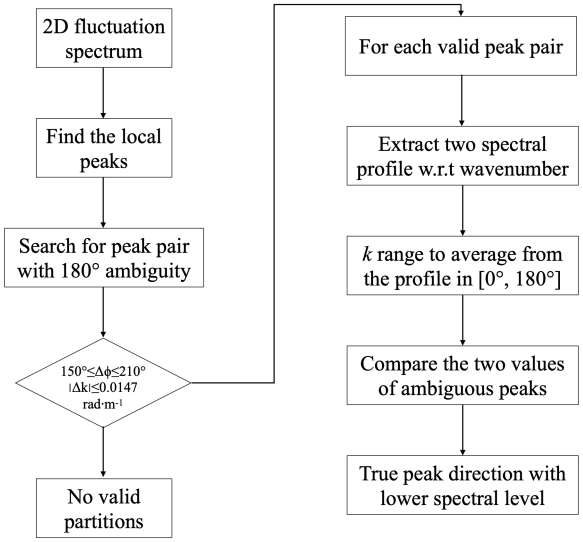

Fig. 6. Flowchart to search for the valid ambiguous peak pairs and to calculate the average of fluctuation spectrum around the identified peaks.

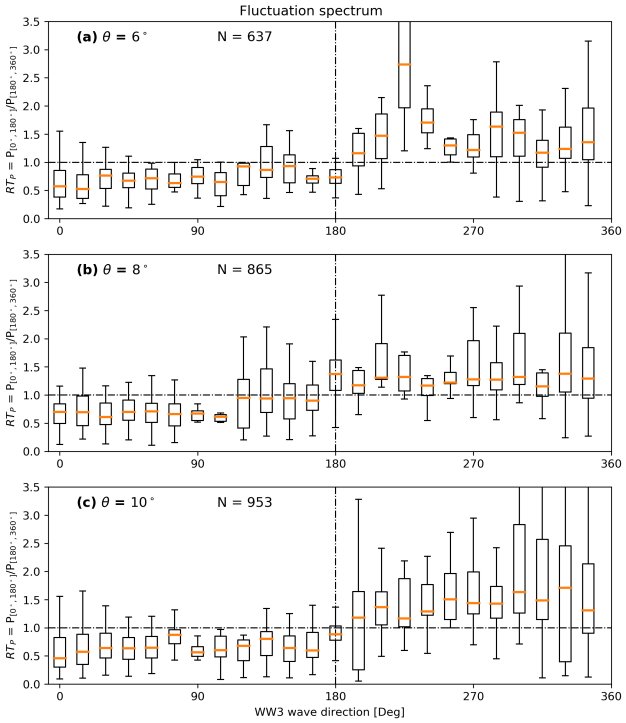

Fig. 7. Box plot of RT_P as defined by Eq. 3 is given regarding the identified WW3 wave peak direction for (a) 6°, (b) 8° and (c) 10° beams. 'N' annotated in each plot denotes the number of valid peak pairs. The lower and higher end of the box are the first (25%) and the third quartile (75%), respectively. The horizontal line within the box represents the median value. Wave direction is relative to the true north (0°) in clockwise rotation. The wave direction bin is 15°.

which confirms the lower fluctuation spectra at downwave direction. In the case of wave direction belonging to [180°,360°], RT_P representing the up-to-downwave ratio is well above the horizontal line of 1. In consequence, it is rational to conclude that the fluctuation spectrum indeed exhibits notable up-to-downwave asymmetry with higher spectral levels at upwave direction.

Note that the distribution of RT_P slightly differs among the three spectral beams. Within the wave direction range of [0°, 180°], the 10° beam shows tighter distribution with its upper interquartile (75% of the points) well below 1. While for both 6° and 8°, the RT_P spans across the horizontal line of one at several wave directions. By contrast, within the wave direction of [180°, 360°], the lower interquartile (25%) of all three spectral beams is mostly above the one line. The behavior that the RT_P spanning on both sides of the one line is expected to introduce biases in applications based on this up-to-downwave asymmetry. In addition, numbers of the identified peak pairs are not the same for the three spectral beams. This is due to the fact that one peak pair is not consistently present in the fluctuation spectrum of the three beams.

We also looked into the RT_P dependence on the relative wave direction in terms of the wind speeds or different peak wavelengths as shown in the APPENDIX. The up-to-downwave asymmetry considering all conditions is also

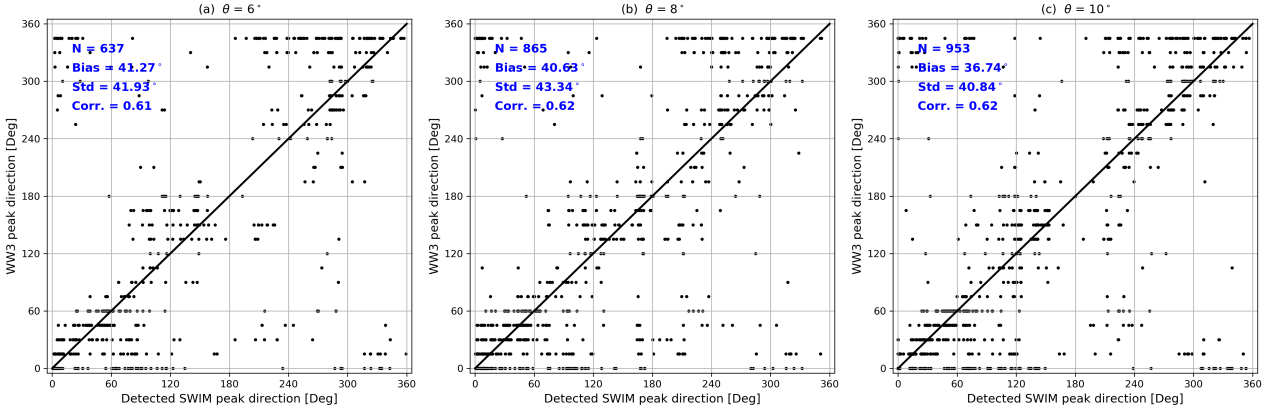

Fig. 8. Comparison of SWIM resolved wave peak direction with respect to the collocated WW3 wave peak direction for (a) 6°, (b) 8° and (c) 10° beams. 'N' annotated in each plot denotes the number of valid peak pairs. Result metrics are given on the upper left corner of each plot.

examined for each category of wind speed ($0 < u_{10} < 5m/s$, $5 < u_{10} < 10m/s$, $10 < u_{10} < 15m/s$) and peak wavelengths ($\lambda_p < 200m$,$\lambda_p > 200m$). There is no clear variation between different wind speeds and the peak wavelengths. Similar trend is observed that RT_P is smaller than 1 for the relative wave direction in the range of [0°, 180°]. In summary, it can be concluded that the up-to-downwave asymmetry of the fluctuation spectrum is solely associated with the relative wave direction. This lays strong basis for the following attempt to remove the wave direction ambiguity by taking advantage of this up-to-downwave asymmetry.

IV. PRELIMINARY RESULTS OF WAVE DIRECTION AMBIGUITY REMOVAL

The RT_P in Fig. 7 illustrates that the fluctuation spectrum at upwave is indeed larger than its counterpart at downwave direction. This characteristics agrees well with the trend of tilt MTF as reported in [18] that it has larger value in the upwave configuration. From the practical point of view, the observed fluctuation spectrum up-to-downwave asymmetry can be readily utilized to help resolve the 180° wave direction ambiguity. As presented in Fig. 7, the downwave direction generally has lower spectral values, which will be taken as the true wave direction. This notation is consistent with the wave direction definition of traveling to in the WW3 products.

In this section, we focus on the wave direction ambiguity removal based on the up-to-downwave asymmetry of the fluctuation spectra. Fig. 8 displays the direction comparison between the SWIM detection results and the collocated WW3 wave spectra for the three spectral beams. It should be noted that the wave slope spectrum is utilized to extract the reference wave peaks. Yet since we use the fluctuation spectrum to identify the spectral peaks, the spectral peak wavelengths might slightly differ with the reference wave peaks derived from the WW3 wave slope spectrum due to the impact of impulse response function and speckle noise spectrum.

As shown in Fig. 8, the extracted SWIM peak directions are in good alignment with the reference WW3 peak direction for all three spectral beams. Acquisitions from both ascending pass and descending pass are included in the analyses, so that the detected SWIM wave directions span in the entire range of [0°, 360°]. It should be reminded that direction comparison demonstrated here are based on the spectral distance criteria of 3 for the peak-to-peak association. The 10° beams in Fig. 8(c) shows the relatively better performance with the smallest direction bias of 36.55° and the standard deviation of 40.61°. By comparison, the 6° beam shows comparable biases and standard deviation with the 8° beam. The better performance of 10° for ambiguity removal is expected based on the tight distribution of the RT_P in Fig. 7. This is consistent with the previously reported results that the 10° is mostly suitable for wave detection [9], [7]. While the correlation coefficient is sort of low, being 0.59, 0.58 and 0.61 for 6°, 8° and 10°, respectively. Combination of the three spectral beams is promising to improve the wave spectral inversion.

Some outliers are still evident, which reduces the quality of direction ambiguity removal. For the 6° beam in Fig. 8(a), a cluster of outliers appears at the position corresponding to the detected SWIM wave direction of 210° and the WW3 wave direction of 150°/60°. The misjudgment of SWIM results can be traced back to the wider spread of RT_P across the horizontal curve of one around the true wave direction of 60° in Fig. 7. Note that the up- and downwave observations are usually 100 km apart, which also might result in errors in the ambiguity removal. In addition, the large scatter around 0° and 360° wave direction is because of the mask close to the track direction. The other wave directions are much cleaner owing to the tight distribution of RT_P. Similar cluster of outliers is observed for the other two beams of 8° and 10° in Fig. 7(b) and (c) as well.

V. DISCUSSION AND CONCLUSION

The concept of a conical scanning real aperture radar operating at near-nadir incidence angles has been proposed and validated using the airborne instruments for decades. With the successful launch of COFSAT, such observations of ocean waves at the global scale are available for the first time ever. Despite the constant effort to update the operational data processing algorithms, the inherent 180° wave direction ambiguity yet hinders some geophysical applications using the SWIM

measurements. In this paper, the up-to-downwave asymmetry of the estimated fluctuation spectrum is first documented. It is worth noting that the fluctuation spectrum over the angular sector of $\pm 15^\circ$ relative to the track direction has been excluded in this analysis due to the high level of speckle noise in this direction. Outside this sector, the mean speckle noise spectrum is subtracted for each incidence beam. The ratio of fluctuation spectrum peaks within $[0^\circ,180^\circ]$ to its ambiguous counterpart within $[180^\circ,360^\circ]$ shows distinct behavior relative to the true wave direction. It can be summarized that the fluctuation spectrum is significantly larger in the upwave than in the downwave direction as shown in Fig. 7. The preliminary results to resolve the wave direction ambiguity in terms of this up-to-downwave asymmetry are promising with relatively better performance of the 10° beam.

This documented asymmetry is consistent with the simulation based on the tilt MTF. At the near-nadir incidence angles, the linear approximation theory relates the modulation spectrum to the wave spectrum via the so-called tilt MTF, which is defined by the change rate of backscattering relative to the incidence angles. Since the wave spectrum can be considered unchanged within the footprint on each side of the SWIM track, under the linear theory, a larger spectrum in the upwave with respect to the downwave can only be explained by a larger MTF in that direction. In [18], the authors analyzed the tilt MTF from an analysis of the backscattering coefficents provided by the Global Precipitation Mission (GPM) . They found that the MTF in Ku-Band and at 10○ incidence is indeed 5 to 10% larger in upwind than in downwind direction for winds between 10 and 15 m/s. Hence, according to the results of [18], the modulation spectrum in downwave should be smaller than that in upwave. This agrees well with the analyses results presented in Fig. 7. The quantitative comparison of such asymmetry yet requires further efforts. For example, the nonlinear range bunching is usually neglected in the state-of-the-art SWIM simulators, which might modify the up-to-downwave asymmetry of the simulated fluctuation spectrum. Other factors including the high-order hydrodynamic modulation and the instrumental performance needs more investigations as well. In any case, this consistent asymmetry shall provide valuable data reference to complete our understanding on SWIM measurement principles.

In addition to the application for direction ambiguity removal, the skewed fluctuation spectrum between upwave and downwave shall be further employed to refine the wave inversion. With the ambiguity resolved and the along-track noise issue corrected, the derived two-dimensional wave spectra shall help to fully characterize the sea state conditions across the globe. More oceanographic studies will benefit from the simultaneous measurements of ocean waves by SWIM and wind field by the scatterometer aboard CFOSAT. For example, the wind-wave interaction can be possibly quantified as well as the local air-sea interaction. Wave in the sea ice is also an promising aspect to investigate, just to name a few.

The preliminary results of ambiguity removal by utilizing the up-to-downwave asymmetry demonstrated in this study are affirmative for the future operational implementation. Though, a more thorough algorithm needs to be devised for quantification of up-to-downwave asymmetry of wave partitions in addition to the local peaks. This algorithm shall greatly help refine the wave inversion scheme as well as enhance the usage of SWIM observations in oceanographic related studies.

APPENDIX

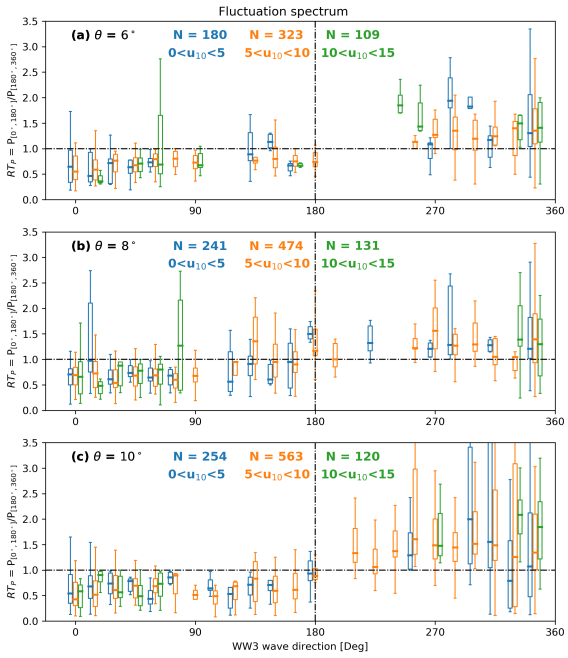

Fig. A1. Box plot of RT_P as defined by Eq. 3 is plotted as a function of the WW3 wave peak direction for three wind speed ranges for (a) 6°, (b) 8° and (c) 10° beams, respectively. 'N' annotated in each plot denotes the number of valid peak pairs.

ACKNOWLEDGMENT

We would like to acknowledge the CNSA and CNES for providing the CFOSAT/SWIM Level-1A and Level-1B products. The ECMWF forecast winds are obtained in the framework of Sentinel-1 Mission Performance and are publicly available (ecmwf.int). WaveWatch III wave spectra are produced at Ifremer/LOPS within the framework of CFOSAT mission. All CFOSAT products are provided by the courtesy of CNSA and CNES.

REFERENCES

[1] Fabrice Ardhuin, Justin E. Stopa, Bertrand Chapron, Fabrice Collard, Romain Husson, Robert E. Jensen, Johnny Johannessen, Alexis Mouche, Marcello Passaro, Graham D. Quartly, Val Swail, and Ian Young, "Observing sea states," *Frontiers in Marine Science*, vol. 6, pp. 124, 2019.

[2] Klaus Hasselmann and Susanne Hasselmann, "On the nonlinear mapping of an ocean wave spectrum into a synthetic aperture radar image spectrum and its inversion," *Journal of Geophysical Research: Oceans*, vol. 96, no. C6, pp. 10713–10729, 1991.

[3] Frederick C. Jackson, W. Travis Walton, and Paul L. Baker, "Aircraft and satellite measurement of ocean wave directional spectra using scanning-beam microwave radars," *Journal of Geophysical Research: Oceans*, vol. 90, no. C1, pp. 987–1004, 1985.

[4] Frederick C. Jackson, W. Travis Walton, and Chich Y. Peng, "A comparison of in situ and airborne radar observations of ocean wave directionality," *Journal of Geophysical Research: Oceans*, vol. 90, no. C1, pp. 1005–1018, 1985.

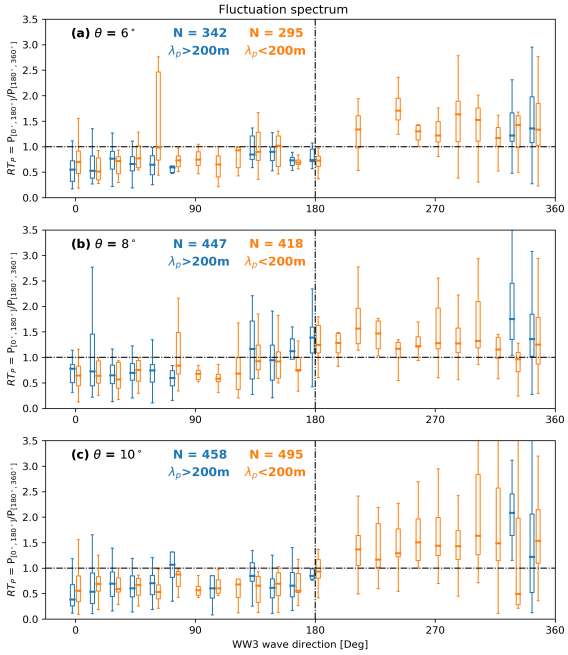

Fig. A2. Box plot of RT_P as defined by Eq. 3 is plotted as a function of the WW3 wave peak direction for two classes of peak wavelength ranges for (a) 6°, (b) 8° and (c) 10° beams, respectively. 'N' annotated in each plot denotes the number of valid peak pairs.

[5] D. Hauser, G. Caudal, G. . Rijckenberg, D. Vidal-Madjar, G. Laurent, and P. Lancelin, "Ressac: a new airborne fm/cw radar ocean wave spectrometer," *IEEE Transactions on Geoscience and Remote Sensing*, vol. 30, no. 5, pp. 981–995, 1992.

[6] Danièle Hauser, Elbatoul Soussi, Eric Thouvenot, and Laurent Rey, "Swimsat: A real-aperture radar to measure directional spectra of ocean waves from space—main characteristics and performance simulation," *Journal of Atmospheric and Oceanic Technology*, vol. 18, no. 3, pp. 421–437, 2001.

[7] Danièle Hauser, C. Tison, T. Amiot, L. Delaye, N. Corcoral, and P. Castillan, "Swim: The first spaceborne wave scatterometer," *IEEE Transactions on Geoscience and Remote Sensing*, vol. 55, no. 5, pp. 3000–3014, 2017.

[8] J. Liu, W. Lin, X. Dong, S. Lang, R. Yun, D. Zhu, K. Zhang, C. Sun, B. Mu, J. Ma, Y. He, Z. Wang, X. Li, X. Zhao, and X. Jiang, "First results from the rotating fan beam scatterometer onboard cfosat," *IEEE Transactions on Geoscience and Remote Sensing*, pp. 1–14, accepted, 2020.

[9] D. Hauser, C. Tourain, L. Hermozo, D. Alraddawi, L. Aouf, B. Chapron, A. Dalphinet, L. Delaye, M. Dalila, E. Dormy, F. Gouillon, V. Gressani, A. Grouazel, G. Guitton, R. Husson, A. Mironov, A. Mouche, A. Ollivier, L. Oruba, F. Piras, R. R. Suquet, P. Schippers, C. Tison, and N. Tran, "New observations from the swim radar on-board cfosat: Instrument validation and ocean wave measurement assessment," *IEEE Transactions on Geoscience and Remote Sensing*, pp. 1–22, 2020.

[10] Kirsty E. Hanley, Stephen E. Belcher, and Peter P. Sullivan, "A global climatology of wind–wave interaction," *Journal of Physical Oceanography*, vol. 40, no. 6, pp. 1263–1282, 2010.

[11] L. Aouf, A. Dalphinet, D. Hauser, L. Delaye, C. Tison, B. Chapron, L. Hermozo, and C. Tourain, "On the assimilation of cfosat wave data in the wave model mfwam : Verification phase," in *Proceedings of the 2019 IEEE International Geoscience and Remote Sensing Symposium*, Yokohama, Japan, 2019, p. ...

[12] L. Aouf, D. Hauser, B. Chapron, A. Toffoli, C. Tourrain, and C. Peureux, "New directional wave satellite observations : Towards improved wave forecasts and climate description in southern ocean," *submitted to Geophysical Research Letters*, 2020.

[13] Gaspar R Valenzuela, "Theories for the interaction of electromagnetic and oceanic waves — A review," *Boundary-Layer Meteorology*, vol. 13, no. 1, pp. 61–85, jan 1978.

[14] C. Cox and W. Munk, "Statistics of the sea surface derived from sun glitter," *Journal of Marine Research*, vol. 13, no. 2, pp. 198–227, 1954.

[15] Michael H. Freilich and Barry A. Vanhoff, "The relationship between winds, surface roughness, and radar backscatter at low incidence angles from trmm precipitation radar measurements," *Journal of Atmospheric and Oceanic Technology*, vol. 20, no. 4, pp. 549–562, 2003.

[16] William J. Plant, "A new interpretation of sea-surface slope probability density functions," *Journal of Geophysical Research: Oceans*, vol. 108, no. C9, 2003.

[17] Ping Chen, Gang Zheng, Danièle Hauser, and Fei Xu, "Quasi-gaussian probability density function of sea wave slopes from near nadir ku-band radar observations," *Remote Sensing of Environment*, vol. 217, pp. 86 – 100, 2018.

[18] Victor Gressani, Frédéric Nouguier, and Alexis Aurélien Mouche, "Wave spectrometer tilt modulation transfert function using near-nadir ku- and ka-band gpm radar measurements," *IGARSS 2018 - 2018 IEEE International Geoscience and Remote Sensing Symposium*, pp. 4107–4110, 2018.

[19] Frederick C. Jackson, "An analysis of short pulse and dual frequency radar techniques for measuring ocean wave spectra from satellites," *Radio Science*, vol. 16, no. 6, pp. 1385–1400, 1981.

[20] Fawwaz T. Ulaby, Richard K. Moore, and Adrian K. Fung, *Microwave Remote Sensing: Active and Passive Volume II*, Reading, Mass. : Addison-Wesley, 1982.

[21] Romain Husson, *Development and validation of a global observation-based swell model using wave mode operating Synthetic Aperture Radar*, Ph.D. thesis, UNIVERSITE DE BRETAGNE OCCIDENTALE, 10 2012.